MCAO testbed for European Solar Telescope (EST): first laboratory results for SCAO and GLAO configurations

Noelia Feijóo*[a], Nicolás Rodríguez*[a], Luzma Montoya[a], Jose M. González-Cava[b], Yolanda Martín[a], Haresh Chulani[a], Miguel Núñez Cagigal[a], Francisco González[a], Jorge Quintero Nehrkorn[a], Ángela Hernández[a]

[a]Instituto de Astrofísica de Canarias, E-38205 La Laguna, Spain; [b]Universidad de La Laguna, E-38206 La Laguna, Tenerife, Spain.

ABSTRACT

A Multi-Conjugate Adaptive Optics (MCAO) testbed has been developed at the Instituto de Astrofísica de Canarias (IAC) as a prototype of the Adaptive Optics (AO) system for the European Solar Telescope (EST). EST is a 4.2-m telescope that will provide high resolution in a 60 arcsec circular Field of View (FoV). For this purpose, EST will be equipped with an MCAO system that will be integrated into the telescope's optical path. The aim of the testbed is to analyse different sensing and wavefront correction strategies in order to check their suitability for EST. The testbed is a downscaled version of the telescope that has been designed to replicate its main features, including the telescope aperture, the FoV and the atmospheric conditions representatives of the telescope site. It allows to set up of Single Conjugate Adaptive Optics (SCAO), Ground Layer Adaptive Optics (GLAO) and MCAO configurations, both for point-like and extended sources. For this purpose, three Shack-Hartmann Wavefront Sensors (SH-WFSs) have been developed and installed in the testbed. A High-Order Wavefront Sensor (HO-WFS) with 33x33 subapertures senses the on-axis 10 arcsec FoV. Additionally, a Multi-Directional WFS (MD-WFS) estimates the turbulence over the entire atmospheric volume. This WFS provides two possible configurations: one high-order spatial resolution (HO-MD-WFS) and another low-order spatial resolution (LO-MD-WFS). A pupil-conjugated deformable mirror (DM) with 820 actuators is currently available for SCAO and GLAO configurations. The introduction of two DMs conjugated to different altitudes will allow the correction of the wide field. The main aim of this contribution is to present the current state of the testbed and the first tests using a Multi-Directional WFS to perform the wavefront reconstruction. The test results show a possible approach to analyse the behaviour of the control loop of an adaptive optics system. It is discussed whether control quality metrics can be used as an alternative to classical optical quality metrics that are especially hard to standardize for solar observation. These metrics are relevant due to the amount of data for GLAO.

Keywords: Testbed; SCAO; GLAO; wavefront sensing; extended field; solar; EST; MCAO.

1. INTRODUCTION

European Solar Telescope (EST) is a 4.2-m solar telescope [1] intended to study the magnetic process between the deep photosphere and upper chromosphere. To this end, it has a set of scientific instruments that can work simultaneously in different spectral ranges between 380 nm and 2300 nm. In order to provide images with high spatial resolution in a 60 arcsec circular Field of View (FoV), EST will correct the effect of the atmospheric turbulence, which is very strong due to daytime observing conditions. This high resolution is achieved thanks to the Multi-Conjugate Adaptive Optics (MCAO) system that the telescope will have integrated into its optical path. This innovative system will be based on atmospheric tomography using WFSs observing different directions within a wide FoV and several deformable mirrors conjugated to different turbulent layers thus correcting the whole atmospheric volume [2]. To study the best strategy in terms of sensing and wavefront correction in EST, a testbed has been developed in the facilities of the Instituto de Astrofísica de Canarias. It is a downscale prototype that simulates the working conditions that the EST MCAO system will have at its site, Roque

de los Muchachos Observatory in La Palma. Some Adaptive Optics (AO) configurations have been proposed to test different sensing and control strategies before introducing a more complex configuration such as MCAO. Good results were obtained with Single Conjugate Adaptive Optics (SCAO) configuration for point sources [3]. The testbed consists of an illumination system centred at 525 nm spectral range providing point-like and extended source capabilities, to which a turbulence simulator is attached. It has a set of three deformable mirrors (DMs), one is a pupil-conjugate DM with 840 actuators and the other two are altitude DMs with 420 actuators each. To perform the tomographic reconstruction, the testbed has two SH-WFSs. One is a narrow field High Order WFS (HO-WFS) and the other one is a wide field Multi-Directional WFS (MD-WFS) with two different resolution configurations [4].

The purpose of this contribution is to present the ongoing advancements in the testbed, focusing on the integration of the subsystems within the AO configurations being tested and their preliminary results. The introduction of the MD-WFS has led to the study of the disturbance rejection behaviour of the system to understand its frequency response and correction capabilities. Some preliminary results were obtained using zonal control.

This document is structured as follows: section 2 provides an overview of the testbed and the AO configurations that have been tested. Section 3 is dedicated to the development of the control scheme used for the tests included in this article. Section 4 proposes a processing technique to analyse the behaviour of the control loop from the frequency response of the slopes. Section 5 presents preliminary results for GLAO and an extended-field image. Finally, in section 6 we summarize our conclusion and future work.

2. TESTBED SET-UP AND CONFIGURATIONS

The MCAO testbed is constituted of several subsystems connected by relay optics. It is highly configurable facilitating transitions between various AO configurations proposed for study and ensuring a high degree of repeatability.

2.1 Subsystems of the testbed

The testbed consists of the following main subsystems:

An *illumination system* comprising two powerful white light sources equipped with a narrow 525 nm filter, which has a bandwidth of 50 nm. These sources are connected to an integrating sphere via two liquid optical fibres, ensuring uniform illumination for all objects. Multiple objects are used to emulate various FoV: a multi-pinhole array with 0.4 arcsec and 0.026 arcsec holes distributed across the 70 arcsec FoV. These two different pinhole sizes are used to achieve the required resolution in the science camera for analyzing the Strehl Ratio across the entire FoV and to maintain an adequate signal-to-noise in the WFS. Additionally, we use two photographic slides, each equivalent to 70 arcsec, which were generated through simulation and developed with the required plate scale and an ideal characteristic contrast of 21%. One is a quiet sun containing solar granulation and another is a large-scale sunspot [4].

The *turbulence simulator* disturbs the image, replicating the atmospheric conditions typical of the telescope site on a scale. It consists of a series of rotating Phase Screens (PS) that allow for the simulation of several vertical atmospheric profiles. There are ten PS available, each with a specific Fried Parameter (r_0), with the capability to integrate five of them simultaneously at different sky equivalent altitudes on the testbed.

The *WFS module* is composed of three pupil-conjugated Shack Hartmann correlation WFSs for atmospheric tomography. The sensing speed is downscaled in a way that the expected sensing speed of 2000 fps at the telescope is transferred to the testbed at 30 fps. A narrow field HO-WFS comprises a 33x33 microlenses array (ML) to provide high spatial resolution sampling of the pupil plane. This WFS measure on-axis turbulence within a 10 arcsec FoV by introducing a field stop in the previous focal plane. A MD-WFS senses a wide 70 arcsec FoV. This WFS has two different configurations depending on the spatial sensing resolution: a Low Order MD-WFS (LO-MD-WFS) with 17x17 subapertures and a High Order MD-WFS (HO-MD-WFS) with 33x33 subapertures. Two different asterisms of 19 or 7 subwindows with 10 arcsec FoV each are implemented in each subaperture. The study of these wavefront sensing alternatives is because current sensors are far from meeting both spatial and temporal requirements defined for a scaled HO-MD-WFS for EST.

The *DMs module* consists of three DMs from ALPAO. A pupil-conjugate DM (DM0) with 820 actuators in a 45 mm diameter is used to correct the high-order turbulence on the ground layer. Additionally, there are two altitude DMs (DM1 and DM2), each with 468 actuators in a 33 mm diameter, which can be conjugated at different altitudes according to the simulated telescope elevation. These two altitude DMs are 45° oriented as in the telescope, which allows us to assess the impact of correcting an elliptical meta-pupil.

The *real-time controller* (RTC) used is DARC [5], developed by Durham University which offers several correlation techniques and real-time response capabilities. As previously mentioned, the testbed has been scaled in temporal frequency so that the PS provide a downscaled dynamic representation of the expected operation conditions for the telescope [6] avoiding a limitation on the cameras'frame rate. Several control strategies can be tested, including modal and zonal control. In terms of controllers, the following options are available in the testbed: a leaky-integrator, Pseudo-Open Loop Control (POLC) [7] or design a custom controller using a Filter-Infinite Impulse Response (FIIR) [8]. Our default controller is a leaky-integrator.

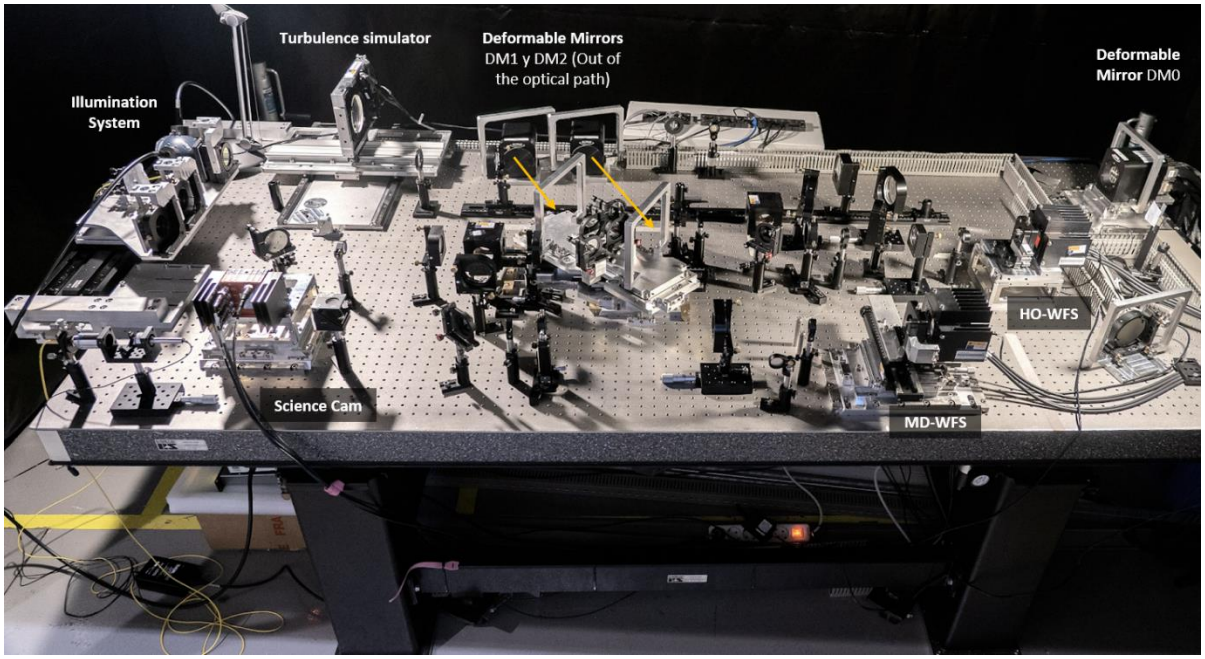

Figure 1. The subsystems that constitute the MCAO testbed.

2.2 SCAO and GLAO configurations

Several AO configurations were proposed for testing with different control strategies prior to the implementation of MCAO, as shown in Table 1. During daytime observations, most of the turbulence accumulates in low layers of the atmosphere, while weak turbulence remains in higher altitudes. Consequently, we employ a HO-WFS to sample within a10 arcsec on-axis FoV, while a low-order sampling is performed using a LO-MD-WFS for wider FoVs, where the turbulence in the high-altitude layer becomes relevant. Another solution that is currently being tested on the testbed involves the use of a single wide-field WFS with high spatial sampling resolution. The use of a HO-MD-WFS is currently valid for testing on the testbed, using a frame rate of 30 Hz. These WFSs are being tested with SCAO, GLAO1 and GLAO2 configurations with a pupil-conjugated DM as a wavefront corrector as specified in Table 1.

The size of each subaperture of narrow field WFS should not be much larger than the isoplanatic angle, while also allowing for the identification of image structures, such as solar granulation in this case, in order to make correlations (Figure 2). Within each 70 arcsec FoV subaperture of the MD-WFS, subwindows with 10 arcsec FoV each are generated by software (Figure 3). This approach allows us to simulate multiple narrow-field WFS pointing in different directions. For wavefront reconstruction, each subwindow within a reference subaperture is correlated with the corresponding subwindow in each

of the other subapertures [9]. Some control strategies were tested for solar SCAO (Figure 2) and GLAO (Figure 3). Better results were obtained using zonal control. The interaction matrix (PMX) was measured with a frequency-based method and the reconstruction matrix (RMX) was obtained by computing the pseudo-inverse of the PMX.

Table 1. Proposed AO configurations to be tested. Those marked in green have already been tested, obtaining some preliminary results.

Configurations						
SCAO	**GLAO1**	**GLAO2**	**MCAO1**	**MCAO2**	**MCAO3**	**MCAO2**
DM0 / HO-WFS	DM0 / HO-WFS & LO-MD-WFS	DM0 / HO-MD-WFS	DM0 / HO-WFS / DM1 / LO-MD-WFS	DM0 / HO-WFS / DM1 & DM2 / LO-MD-WFS	DM0 & DM1 / HO-MD-WFS	DM0 & DM1 & DM2 / HO-MD-WFS

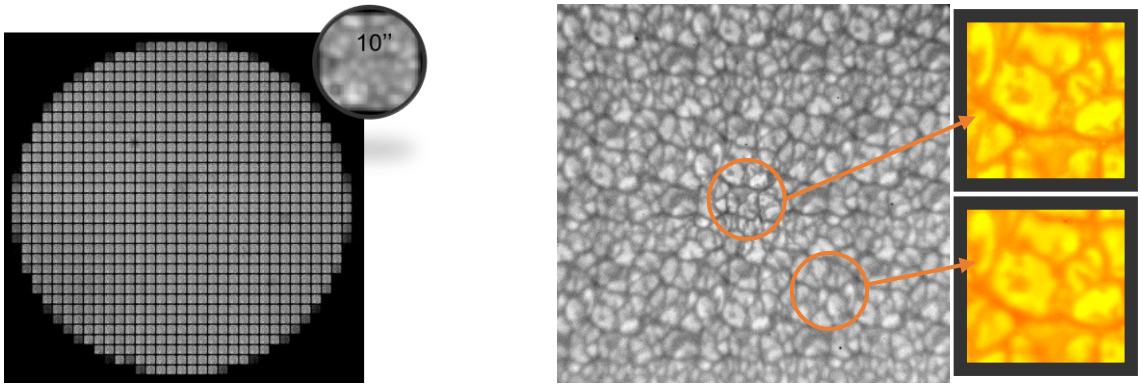

Figure 2. Raw image of narrow field HO- WFS (left) and corrected image using SCAO with turbulent layers at 0km and 40 km with r_0 (λ525 nm) 10 cm and 36 cm respectively (right). Some areas of great interest due to their magnetic activity appear resolved in a 10 arcsec FoV.

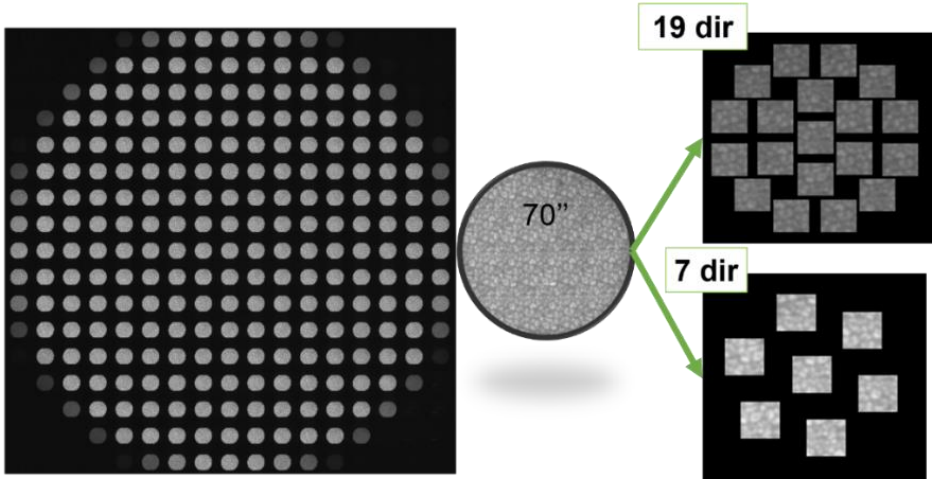

Figure 3. Raw image of the LO-MD-WFS and both possible asterisms.

3. CONTROL METHOD

Currently, the control loop implemented in the testbed is a disturbance rejection scheme, in which the disturbance introduced by the phase screens (atmosphere) is rejected. Figure 4 shows the block diagram of the loop when correlations are used.

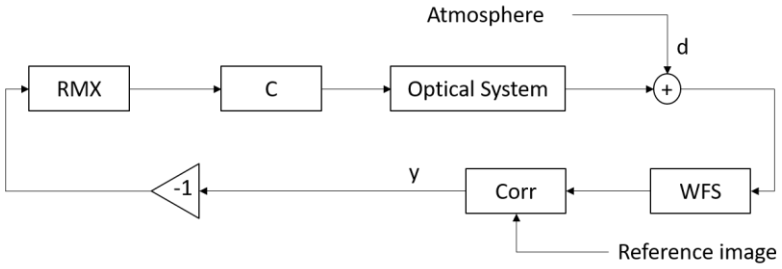

Figure 4. Zonal control loop.

In the previous diagram, the Optical System includes the dynamics of the DMs. WFS and Corr blocks correspond to the wavefront sensor and the correlation algorithm, which introduce processing delay within the loop.

The system output y can be expressed as a function of the disturbance d using the sensitivity function S, as shown in equation 1:

$$y = \frac{Corr * WFS}{I + Corr * WFS * Opt.* C * RMX} \cdot d = S \cdot d \tag{1}$$

The sensitivity transfer function is useful for characterizing the frequency-domain rejection of the control loop, as well as for measuring the performance and robustness of the system. Therefore, the main approach for studying the loop response relies on identifying this matrix from experimental data.

In the testbed, the problem of knowing the input disturbance can be skipped by measuring in open loop the slopes when the phase screen is in motion and a flattened DM is in the system as depicted in Figure 5. Then, the output of the system is acquired by measuring the slopes in closed loop.

Figure 5. Input disturbance measurement.

As we are aiming to obtain a frequency response, the output and disturbance signals will be expressed as Power Spectral Density (PSD), which leaves the expression in equation 2:

$$|S(f)| = \sqrt{PSD(y) \cdot PSD(d)^{-1}} \tag{2}$$

The input disturbance of the atmosphere measured in one subaperture can be considered independent and decoupled from the disturbance measurement in the remaining subapertures. Nonetheless, each actuator will affect several subapertures, and this effect cannot be compensated. The reconstruction matrix minimizes the coupling by using weights depending on the intensity of the interaction. However, the weights do not fully decouple the system when there are multiple control objectives (slopes to nullify) in a local area and the ideal individual control action can interfere with each other. For this

case, the response of the control loop will be a sort of average control action for the local area, reaching a certain equilibrium that minimizes the overall error in the region.

This interaction effect is more noticeable for the subwindows within one subaperture. For the HO-MD-WFS which has 33x33 subapertures, one actuator potentially affects all subwindows within each subaperture. In fact, this relation between each actuator and all subwindows is a controllability problem limiting GLAO capabilities, especially when the specific weight of altitude layer is relevant with respect to the ground layer. MCAO is a solution to this controllability problem.

A priori, the interaction effect does not impact the sensitivity analysis. Our goal is to understand the rejection behaviour of our system in each region of the pupil. The interaction is important for diagnosing the causes of not reaching better performance, but is not a part of the analysis itself.

Following this reasoning, we will study the system with a one-to-one correspondence between the disturbance measurement in one subwindow and the output in closed loop at the same subwindow.

The drawback of the previous approach is that we have multiple sensitivity functions, which are hard to evaluate as a whole. To address this problem, data science techniques are important to reduce the complexity of the information and obtain global metrics.

4. PROCESSING

In this section, an overall description of the processing proposed is done. The analysis starts with the temporal series of input disturbance and output residual. These series are processed to obtain their PSD that are defined for the range 0 to 15 Hz.

After obtaining the PSD of each subwindow, equation 2 is employed to compute the magnitude of the sensitivity function. The highest and smallest values of the magnitude will determine the behaviour of each subwindow. The general objective for disturbance rejection loops is to obtain a response in which the highest value occurs at high frequency, having a wide rejection band. Additionally, the highest value defines the robustness of the system, in which higher values imply less robustness.

However, in the system there are more than 11,000 responses, corresponding to the number of subwindows per subaperture and the number of subapertures used. This generates an incredible amount of data to be analysed, making it difficult to find a good procedure to evaluate the response of the system in terms of slopes behaviour.

Furthermore, it is common during a long execution to have some slopes taking high values due to illumination problems, phase screen local defects, failure of the correlation algorithm, etc. These high values will affect the frequency response, as can be seen in Figure 6 for a local set of subapertures.

Therefore, it is key to pre-process the data to remove outliers. There are two main approaches for this step, one involves detecting and removing outliers from the temporal sequence of measurements, while the approach followed in this section is based on the frequency domain response and the optical information properties of the light at the pupil plane.

In order to reduce the complexity related to the number of existing sensitivity functions, we propose to average these functions as an initial approach. The averaging was performed by splitting based on direction and axis, resulting in the acquisition of 14 magnitude responses.

Before computing the average, it is important to remove outliers, which was done using median absolute deviation (MAD) as a metric to discard data points.

Figure 7 illustrates the behaviour of the average sensitivity transfer function, while in Figure 8, we can see the average of each direction with the standard deviation. The general behaviour of each direction and coordinate is that of a typical sensitivity function. Moreover, the typical deviation shows that the response of the subapertures is close in terms of

frequency rejection, as the internal is fitted to the average. This implies that the frequency response of the subapertures is closely related, something expected as the controller gains and decay used is common.

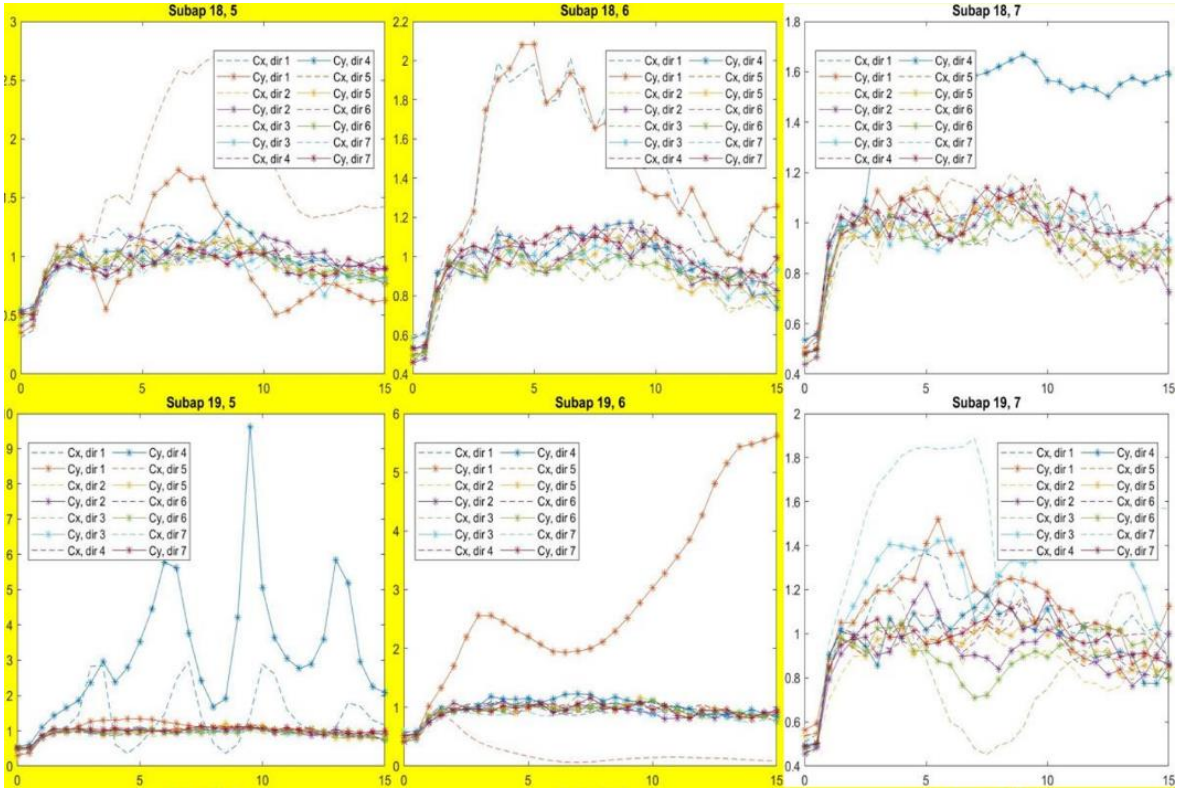

Figure 6. Sensitivity functions zooming at a region of the pupil, without pre-processing.

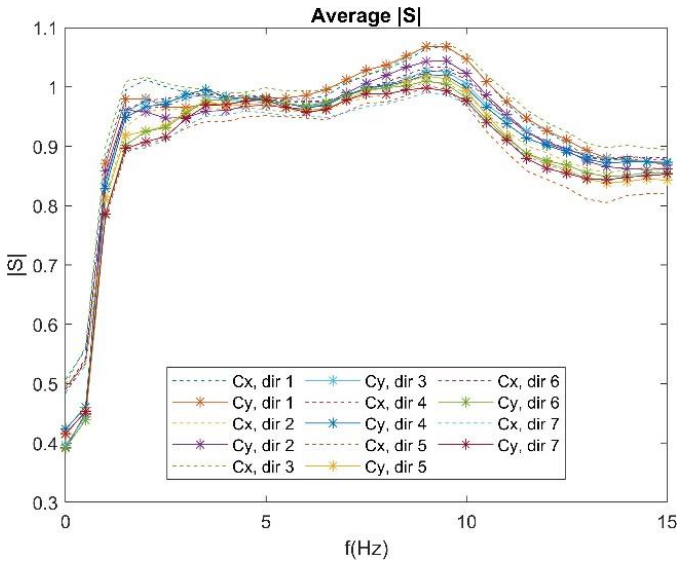

Figure 7. Average sensitivity function.

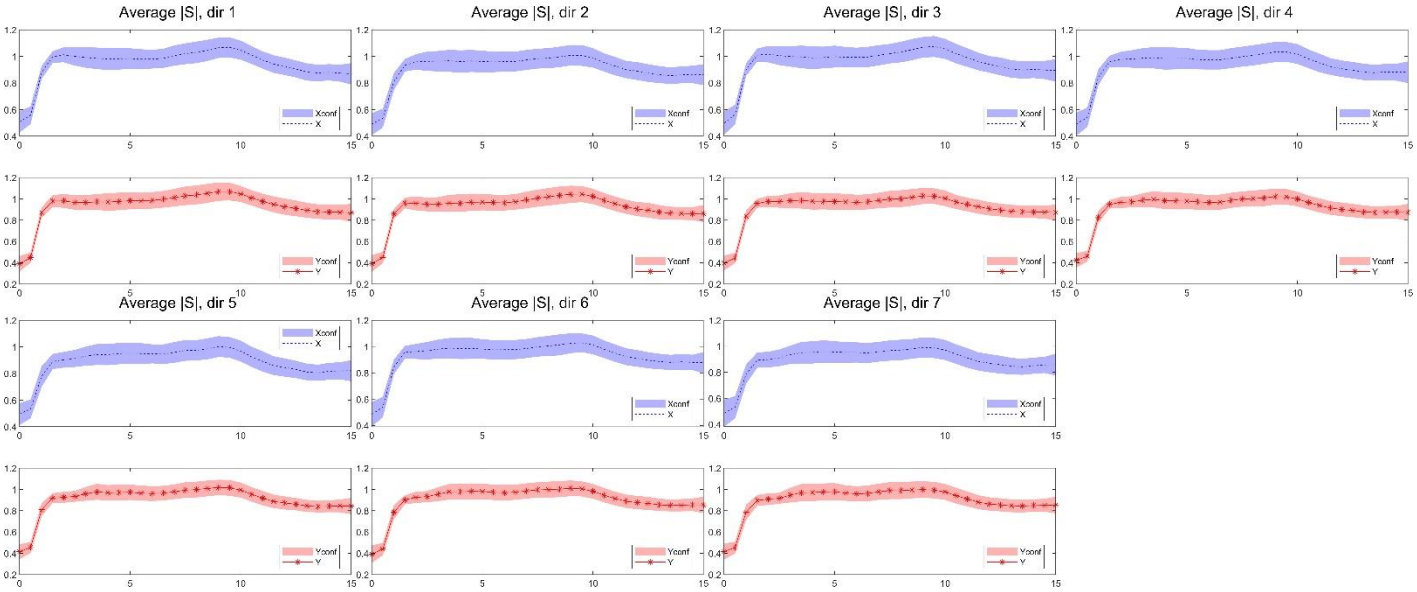

Figure 8. Average sensitivity function with standard deviation.

5. PRELIMINARY RESULTS

In this section, it is performed an analysis of the results obtained during an extended-field test, working with an image of the sun. The correlation method used is based on square-differences to generate the correlation image and a parabolic fitting to find the correlation point with a subpixel precision. A PS of r0 10 cm was located at 0km, rotating at 0.3 rpm which is equivalent to a wind speed of 10 m/s.

The recorded temporal sequences consist of 5400 samples, with a sampling rate of 30 Hz, equivalent to one full turn of the phase screen. Two different asterisms will be analysed, one with 7 directions and another one with 19 directions. The tuning criteria employed aim to maintain a stable loop behaviour throughout the full sequence and avoid actuator saturation. Therefore, loop performance was limited.

For both cases, the contrast obtained in the science camera was 0.11 in open loop, improving it to about 0.15 closing the loop (Figure 9). By adjusting the tuning to allow the sporadic saturation of some actuators, it could be improved to 0.17. However, the maximum contrast of the system, without phase screens, was 0.21.

During the tests performed, we identified two parameters that can affect the stability of the system, apart from the controller gain and decay. On the one hand, in order to reduce computational load, we compute only the central pixels of the correlation image. However, reducing the matching area increases the probability of not matching the patterns and obtaining an incorrect parabolic fitting. On the other hand, as a previous step, we measure the interaction matrix of the DM with the WFSs, which is then inverted to obtain the reconstruction matrix that is used in the control loop. During the pseudo-inversion it is common to filter the singular values to avoid numerical issues and reduce high frequency noise using a threshold (rcond) that has proved to impact the stability of the system and the number of incorrect measured centroid values.

Considering that each subwindow has 25 píxeles and subtend 10 arcsec, increasing the correlation clip by 2 pixels on each side of the square subaperture leads to 2% more centroids lost, while increasing the filtering threshold from a 2.5% of the highest singular value to a 5% reduces the centroids lost by a 2.5 %. This behaviour is coherent with our previous SCAO tests [3].

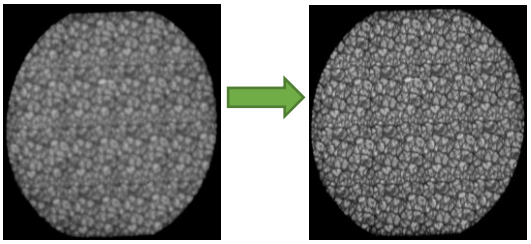

Figure 9. A blurred image due to a turbulence layer at 0km with r_0 ($\lambda 525$ nm) of 10 cm (bottom left) and a wide FoV corrected image closing the loop with GLAO.

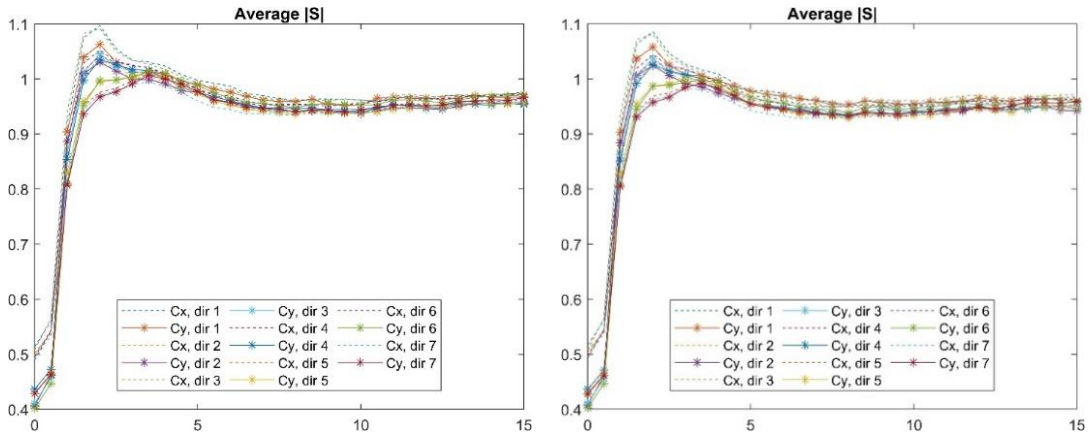

Figure 10. Avrg. Sensitivity function, 7 directions, corrClip 8, rcond 0.025(left)-rcond 0.05 (right).

Figure 10 shows that increasing the rcond parameters does not impact excessively the behaviour of the sensitivity function, which implies that the rejection is kept. The removal of singular values simplifies the interaction mapping but can deteriorate the overall loop performance. However, the noise introduced during the interaction matrix measurement might create problems during the matrix inversion, necessitating the removal of singular values to mitigate this effect. This parameter should be tuned so that the frequency response is not affected while reducing the number of incorrectly measured centroid values.

In Figure 11, we can compare the behaviour of the loop when 19 directions are used instead of 7 directions. The rcond and correlation parameters are equivalent to those in Figure 10 (left), but the controller was tuned to guarantee stability. For 7 directions, a gain of 0.1 and a decay of 0.9 were used, while for 19 directions, the gain was kept constant and the decay was reduced to 0.855.

It can be seen that the peak of the sensitivity function is reduced when using 19 directions, increasing the robustness of the system. However, at low frequencies, the rejection performance deteriorates, which in the temporal domain is directly related to the presence of an offset in the error. This offset is reduced when using 7 directions. This phenomenon can be attributed to the GLAO configuration, where one actuator of the pupil-conjugate DM corrects all the directions.

The optical quality achieved during the tests could not be further improved beyond the contrast level mentioned at the beginning of this section. We have identified three error sources: references reliability, excessive centroids lost and interaction limitation.

We are currently working on these problems to improve our results before beginning with MCAO configurations, where we expect more interaction problems.

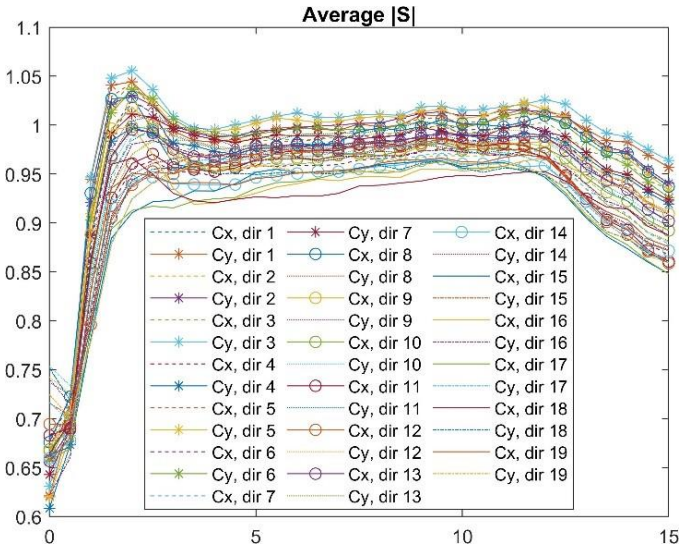

Figure 11. Avrg. Sensitivity function, 19 directions, corrClip 8, rcond 0.025.

6. CONCLUSIONS AND FUTURE WORK

In this article, the MCAO testbed for the EST has been introduced. We have addressed the problem of GLAO, working with extended object images, and its implications in the amount of data and its difficulty in performing data reduction.

We propose a technique to analyse the frequency response based on slope behaviour, with the aim of providing a new approach for developing metrics to assess robustness, increasing the tools to improve the controller. This is relevant for solar images, as we do not have a sensitive quality metric such as Strehl Ratio, but it could also be helpful for night observation as the frequency response gives more information for the tuning process than the Strehl Ratio, which is a magnitude metric.

However, the results obtained do not meet the expected results in terms of image quality, control stability and rejection behaviour. The results obtained lead us to evaluate some paths for improvement: the optical quality of the testbed, the repeatability of the reference measurement and the stability of the measurement of the slope, dealing with the loss of centroids before computing the control signal.

After improving the base behaviour of the system, we will study in depth the interaction observed between directions and actuators, and the impact that it has in the maximum error correction that can be achieved. The interaction is known to be solved by MCAO configuration.

Lastly, we expect to extend this analysis to modal control, in which frequency response might give us more information while reducing the complexity of the measurements.

ACKNOWLEDGMENTS

This work was supported by the EST Project Office, funded by the Canary Island Government (file SD 17/01) under a direct grant awarded to EST on ground of public interest.

REFERENCES

[1] Quintero Noda, C., et al., “The European Solar Telescope,” Astronomy & Astrophysics, 666, A21

[2] Montoya, L. M., Velasco, S., Sánchez-Capuchino, J., Collados, M., et al., “The real time MCAO solar prototype for the EST,” Proc. SPIE 10703, 1155-1160 (2018).

[3] González-Cava, JM., Chulani, H., Martín, Y. et al., “Laboratory results of SCAO: getting ready for the EST MCAO,” Proc. SPIE 12185 (2022).

[4] Feijóo, N., González, F., Montoya, L.M., et al., “Optomechanical integration of the MCAO prototype testbed for EST,” Proc. SPIE, 12185 (2022).

[5] Basden, A. G., Geng, D., Myers, R., Younger, E. “Durham adaptive optics real-time controller,” Applied Optics, 10, 6354-6363 (2010).

[6] Femenía Castella, B., Montoya, L. M., García, I. M., et al. “Adaptive Optics at the European Solar Telescope: status and future developments,” Proc. SPIE 12185 (2022)

[7] Piatrou P, Gilles L., “Robustness study of the pseudo open-loop controller for multiconjugate adaptive optics”, Applied Optics, 44, 1003-1010 (2005).

[8] Agapito, G., Arcidiacono, C., Quirós-Pacheco, F., Puglisi, A., Esposito, S. “Infinite impulse response modal filtering in visible adaptive optics,” Proc. SPIE 8447, (2012).

[9] Schmidt, D., Berkefeld, T., Heidecke, F., von der Lühe, O., and Soltau, D. “Testbed for the multi-conjugate adaptive optics system of the solar telescope GREGOR,” Proc. SPIE 7439 (2009).